www.czasopisma.pan.pl PAN POLSKA AKADEMIA NAUK www.journals.pan.pl

Arch. Metall. Mater. **67** (2022), 4, 1455-1458

DOI: https://doi.org/10.24425/amm.2022.141073

MOHAMED AFQIR[1*], MOHAMED ELAATMANI[1], ABDELOUAHAD ZEGZOUTI[1], NABIHA TAHIRI[1], MOHAMED DAOUD[1]

STRUCTURE AND DIELECTRIC PROPERTIES OF V AND Y DISORDER DOPED $SrBi_2Nb_2O_9$ CERAMICS

Y and V codoped $SrBi_2Nb_2O_9$ ceramics, which have been characterized by XRD, FTIR and SEM techniques, were prepared through molten salt using NaCl-KCl medium. Through X-ray diffraction analysis, all prepared samples were matched by undoped $SrBi_2Nb_2O_9$. The lattice parameters do not depend on the amount of dopants. Under the optimized experimental conditions, the compounds are composed of small crystallites of varying size and orientation, resulting in many micros train defects. FTIR spectra revealed that the dopant promotes a slight decrease in the 612 cm^{-1} band. A plate-like morphology was revealed by scanning electron microscopy, while Nyquist plots indicate non-Debye relaxation for all compounds. V and Y were incorporated into $SrBi_2Nb_2O_9$ lattice in order to reduce dielectric loss tangent. Thus, the codoping increases the of $SrB_{1.9}Y_{0.1}Nb_{1.95}V_{0.05}O_9$ (Y0.1V0.05) ceramic whereas, they were significantly decreased in the case of $SrBi_{1.8}Y_{0.2}Nb_2O_9$ (Y0.2) ceramic. Y0.1V0.05 sample makes up the highest efficient charge transfer, followed by Y0.2 sample representing the lowest.

Keywords: Molten salt method; Co-doping; Characterization

1. Introduction

Aurivillius structures were first studied by B. Aurivillius in 1949. These types of materials present a laminar structure, $(Bi_2O_2)^{2+}(A_{n-1}B_nO_{3n+1})^{2-}$, where A and B are the cations that form pseudo-perovskite $(A_{n-1}B_nO_{3n+1})^{2-}$ interleaving between the bismuth oxide layers, $(Bi_2O_2)^{2+}$ [1]. Fatigue-free properties allowed $SrBi_2Nb_2O_9$ such as $SrBi_2Ta_2O_9$ to be the best candidates for nonvolatile memory devices [2-4].

So far, doping and synthesis strategy remain the two principal concerns in order to improve physical properties. Materials based on $SrBi_2Nb_2O_9$ have been synthesized through several methods such as coprecipitation, solid-state, hydrothermal, epitaxial [5]… etc. Molten salt of materials was synthesized by solid-state where the salt is added to the reactants and heated above the eutectic point of the salt [6-7]. Because of the complexity of $SrBi_2Nb_2O_9$ synthesis, the molten salt technique has not been extensively used to prepare $SrBi_2Nb_2O_9$ materials. Bao-rang Li et al. have been reported that the pure $SrBi_2Nb_2O_9$ powders could be obtained at a temperature higher than 700°C by molten salt synthesis using KCl medium [8].

The effect of doping of $SrBi_2Nb_2O_9$ ceramics has been widely discussed in the literature and is now in progress. We reported recently that the replacement of Bi by rare earth elements reduces dielectric loss tangent and decreases the Curie temperature. Meanwhile, the electronic configuration of Nb atoms has an effect on ferro-piezoelectric, magnetic and conduction, similar to those presented in the perovskite structures. The dielectric properties of $SrBi_2Nb_2O_9$ ceramics were found to be enhanced by the partial replacement of Nb ions by pentavalent vanadium ions [9]. Moreover, Susan M. Blak et al. have reported that for $SrBi_2Nb_2O_9$ (A = Ba, Sr, Ca) the orthorhombic distortion increases with decreasing A^{2+} cation size and originates from the bonding requirements at the perovskite A site [10]. Within partial substitution of Sr^{2+} by Bi^{3+} would increase the Curie temperature and improve the dielectric properties in $SrBi_2Nb_2O_9$.

This work highlights three points. First, $SrBi_2Nb_2O_9$ ceramics doped with yttrium and vanadium were obtained using the molten salt method. Second, the characterization of prepared samples was carried out. Third, dielectric properties at room temperature were discussed.

2. Experimental

To carry out the Y and V co-doped $SrBi_2Nb_2O_9$ (TABLE 1) by the molten salt method. First, $SrCO_3$, Nb_2O_5, Y_2O_3, Bi_2O_3 and NH_4VO_3 were ground in stoichiometric amounts. After that,

[1] UNIVERSITÉ CADI AYYAD, FACULTÉ DES SCIENCES SEMLALIA, LABORATOIRE DE SCIENCES DES MATÉRIAUX ET OPTIMISATION DES PROCÉDÉS, MARRAKECH, MOROCCO

* Corresponding author: mohamed.afqir@yahoo.fr

© 2022. The Author(s). This is an open-access article distributed under the terms of the Creative Commons Attribution-NonCommercial License (CC BY-NC 4.0, https://creativecommons.org/licenses/by-nc/4.0/deed.en which permits the use, redistribution of the material in any medium or format, transforming and building upon the material, provided that the article is properly cited, the use is noncommercial, and no modifications or adaptations are made.

Bi_2O_3, 10 w% ratios, was added to the mixture to compensate for the bismuth loss during the sintering process. Next, salt KCl-NaCl was added as solvents in a 50/50 w% ratio. Both salts and precursors were mixed then heated at 700°C for 2 hours.

The resulting samples were washed several times with water in order to eliminate chlorides remaining in the material. The resulting powder was dried, then calcined at 1000°C for 12 hours. Pellets (φ 6 mm×1 mm) were prepared by cold hydraulic pressing at 200 MPa, and sintering was carried out at temperature 1120°C for 15 hours. Silver electrodes were deposited on pellets by firing silver paste at temperature 400°C during the 1 hour to form a parallel plate capacitor.

Samples were characterized through Bruker D8 X-ray diffraction equipment, VERTEX 70v FT-IR Spectrometer, Spectrometer UV-2550 (Shimadzu), TESCAN Scanning Electron Microscope and Solartron 1260 impedance/gain-phase analyzer.

TABLE 1

Summary of samples notation

Chemical formula	Y content	V content	Sample notation
$SrBi_2Nb_2O_9$	0	0	$SrBi_2Nb_2O_9$
$SrBi_2Nb_{1.8}V_{0.2}O_9$	0	0.2	V0.2
$Sr_2Bi_{1.95}Y_{0.05}Nb_{1.9}V_{0.1}O_9$	0.05	0.1	Y0.05V0.1
$Sr_2Bi_{1.9}Y_{0.1}Nb_{1.95}V_{0.05}O_9$	0.1	0.05	Y0.1V0.05
$Sr_2Bi_{1.8}Y_{0.2}Nb_2O_9$	0.2	0	Y0.2

3. Results and discussion

Fig. 1 shows XRD spectra of undoped and doped $SrBi_2$-Nb_2O_9 ceramic powders. All samples are matched by SBN JCPDS (card No. 01-089-8154). As can be seen, there is no difference significant between the reflections of the main patterns of pure and doped samples except Y0.2 sample, a split peak appears (which is marked by *). This split peak is observed at $2\theta = 29.5°$, corresponding to the strongest (115) plane reflection,

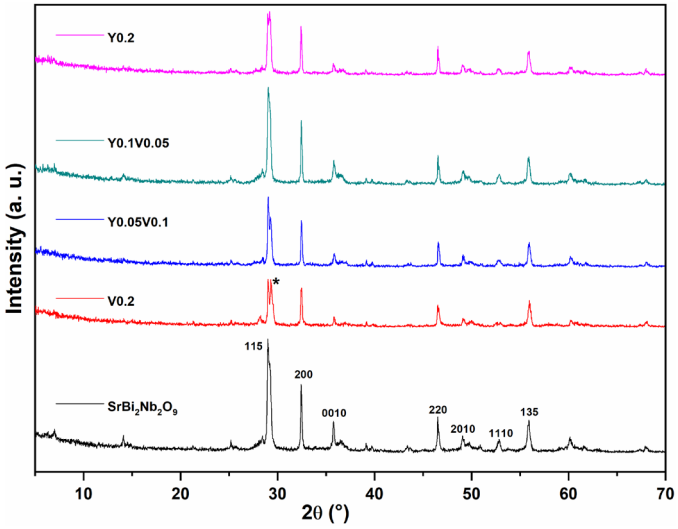

Fig. 1. XRD spectra of $SrBi_2Nb_2O_9$, and doped $SrBi_2Nb_2O_9$ ceramic powders

which looks like K-alpha_2 radiation. This peak splitting could be at the first time assigned to another crystal phase leading to a lower symmetry. However, for the X-ray diffraction pattern, splitting peaks could be attributed to the experimental conditions of the sample. Annealing conditions maybe not be optimized to disappear the overlapping of peaks. Thus, we can deduce that splitting the XRD peak of the Y0.2 sample indicates the low degree of crystalline perfection that could be attributed to the calcination treatment which is a cause of hampering the crystallinity and homogeneity of the samples considerably.

Taking the intense isolated well-defined peaks, Fig. 2(a) shows crystallite size for each (h k l) reflection peak. The values of crystallite size have varied between 10 nm and 90 nm for all samples. Two outlier values of crystallite size were raised at (2 0 0) reflection and (2 2 0) reflection for $SrBi_2Nb_2O_9$ and Y0.2 respectively. In spite of the outlier, there is a smooth significant difference in crystallite size values, which indicates a similar crystallinity for all samples.

Fig. 2(b) shows a scatter plot of microstrain as a function of (h k l) reflection. The microstrain values have varied between 0.05% and 0.9% for all samples. The higher values of microstrain could be raised by dislocation defects. Based on scattering values of microstrain reported in Fig. 2(b), the assumption of homogeneity and isotropy is not obtained.

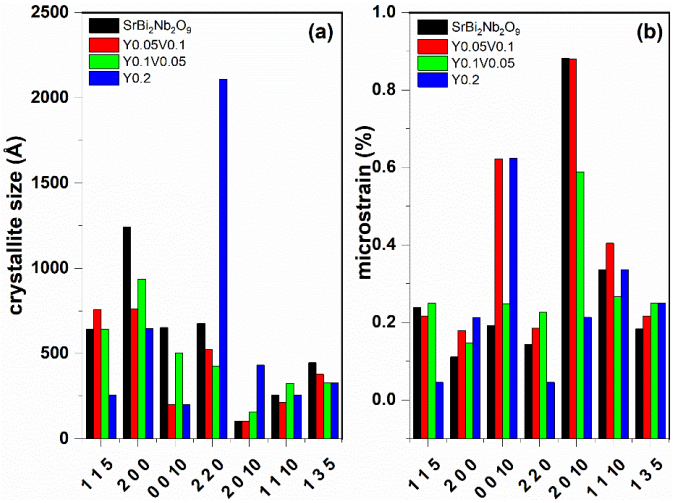

Fig. 2. (a) crystallite size and (b) microstrain values for each (h k l) reflection peak

Lattice parameters as a function of prepared samples are shown in Fig. 3. The resultant lattice parameter for the undoped sample is in good agreement with the values cited in JCPDS (card No. 01-089-8154). Depending on the ionic radius of either dopant, the lattice parameters increase or decrease with increasing or decreasing the amount of dopants. The linearity is not respected; the regression is under-fitted and has not accurately modeled the relationship between lattice parameters and the amount of dopants.

The functional groups of undoped and doped $SrBi_2Nb_2O_9$ compounds are given by comparison of FTIR spectra (Fig. 4). For undoped $SrBi_2Nb_2O_9$, bands were observed around 431.90

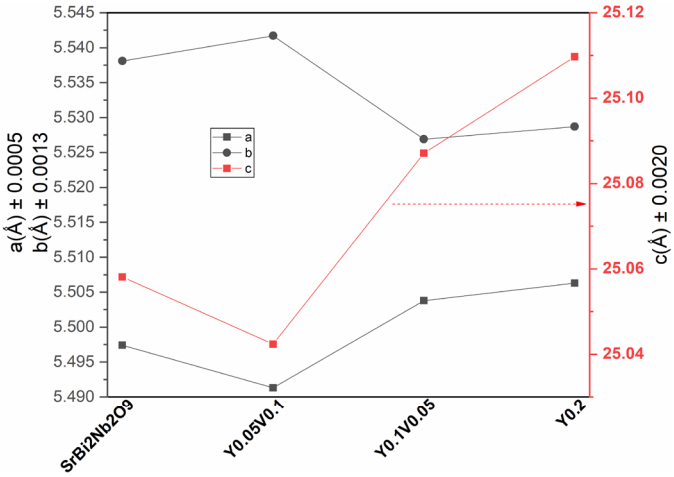

Fig. 3. Lattice parameters of $SrBi_{2-x}Y_xNb_{2-y}V_yO_9$ ($0 \le x \le 0.2$ and $0 \le y \le 0.2$)

and 612.36 cm^{-1}. The strong band around 612 cm^{-1} is characteristic of the Aurivillius family, it may be assigned to the vibrations of Nb-O bonds. Normally, the wavenumber 612.36 cm^{-1} was expected to get shifted towards the higher wavenumber region after the V doping Nb site because of the reduced effective mass of the Nb-O bond. However, our results don't appear to be conclusive, it may be due to the incorporation of two elements Y and V into $SrBi_2Nb_2O_9$ structure involving lower wavenumber.

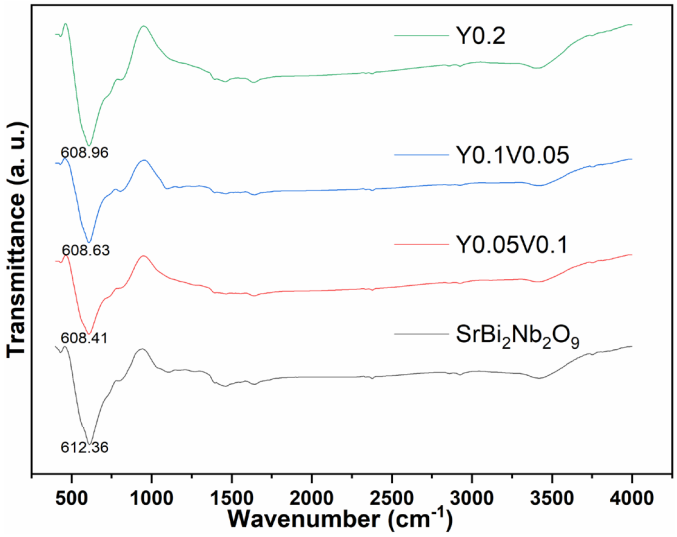

Fig. 4. FTIR spectra of of $SrBi_{2-x}Y_xNb_{2-y}V_yO_9$ ($0 \le x \le 0.2$ and $0 \le y \le 0.2$)

Fig. 5 shows the morphology of the heat-treated $SrBi_{2-x}Y_xNb_{2-y}V_yO_9$ ($0 \le x \le 0.2$ and $0 \le y \le 0.2$) ceramics. In all photographs, the platelet-like morphology of Aurivillius-type compounds is evident. The samples did not show delamination that usually occurs when this type of compound is prepared by the solid-state method [11]. The fact that all the microstructures are similar in nature showing plate-like bonded structures may be explained by the molten salt process did not lead to apparent changes in shape and size of the particles. However, for ceramic doped only by yttrium (Y0.2), the shape of a plate-like well-defined is appeared in the smaller region (red circle) with grain dimensions of 3 μm and 0.89 μm for length and thickness respectively. The average plate thickness was 0.83, 0.75 and 0.13 μm for undoped, Y0.1V0.05 and Y0.05V0.1 ceramics respectively. Based on this result, the plate thickness is decreased as a result of large amounts of vanadium released in the compound.

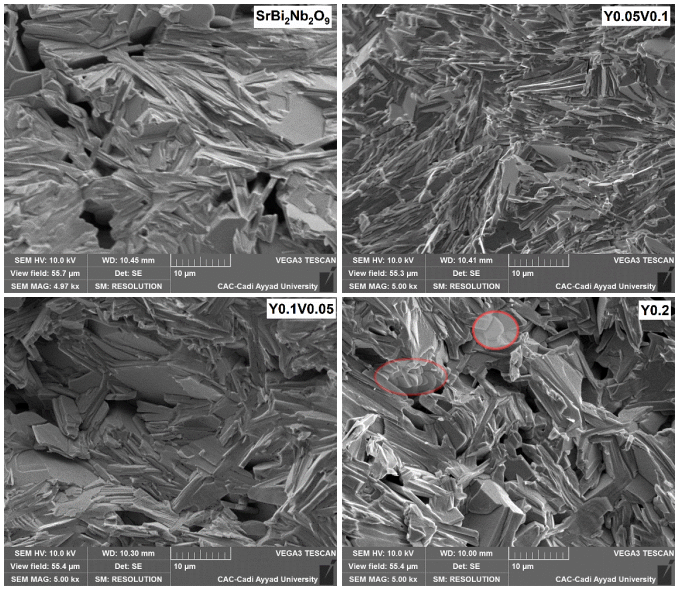

Fig. 5. SEM images of $SrBi_{2-x}Y_xNb_{2-y}V_yO_9$ ($0 \le x \le 0.2$ and $0 \le y \le 0.2$) ceramics

Dielectric constant (ε') and dielectric loss tangent ($\tan\delta$) as a function of frequency, at room temperature for undoped and doped ceramics are presented in Fig. 6. The effect of doping is more pronounced at low frequencies. Above 10^4 Hz, the samples show a lower dependence on the constant dielectric with frequency. At 10^5 Hz, the dielectric constant values have reached 123.5 for V-doped $SrBi_2Nb_2O_9$ ceramics, which are higher than

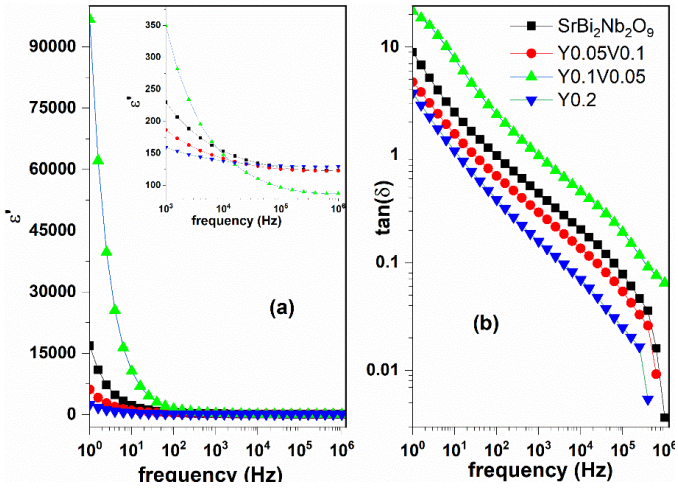

Fig. 6. (a) dielectric constant (ε') and (b) dielectric loss tangent ($\tan\delta$) as a function of frequency, at room temperature of $SrBi_{2-x}Y_xNb_{2-y}V_yO_9$ ($0 \le x \le 0.2$ and $0 \le y \le 0.2$) ceramics

for those of Y0.1V0.05 and Y0.2 ceramics. Regarding dielectric loss tangent, the lowest values in the 10^4 Hz÷1 MHz frequency range for all samples. However, at a lower frequency, a high dielectric loss tangent of about 2.1 was found it. The origin of dielectric loss can be attributed to different processes such as: electric conductivity, ion hop, dipole relaxation, Distortion of network and ion vibration [12]. These processes could be attributed principally to charge carriers that accumulate near the charged electrodes. The highest dielectric loss tangent values are obtained for the Y0.1V0.05 sample. The values of dielectric loss tangent are higher for undoped ceramic compared to the Y0.2 sample.

Qualitatively analyzing the Nyquist diagram (Fig. 7), a significant qualitative irregularity is observed in all samples. All materials follow the typical behavior of a dielectric, being resistive at low frequencies and capacitive at high ones [13]. The compounds have one electroactive zone which its equivalent circuit can be assembled of two elements in parallel, resistance and CPE (constant phase element). The resistance and capacity values of the arches associated were indicated on the inset Table (Fig. 6). Generally speaking, except for one sample Y0.1V0.05, all samples have an arc representing a grain contribution in the specimens which indicates non-Debye relaxation and an insulator behavior [14-15]. Herrin, Y0.1V0.05 sample gives rise to higher charge transfer due to its small radius semicircle and therefore this charge transfer is suppressed in the case Y0.2 sample. Charge transport is not only understood in terms of a potential barrier caused due to charge transfer between the grain boundary and the grain, but also on several factors such as doping level of the material and defects.

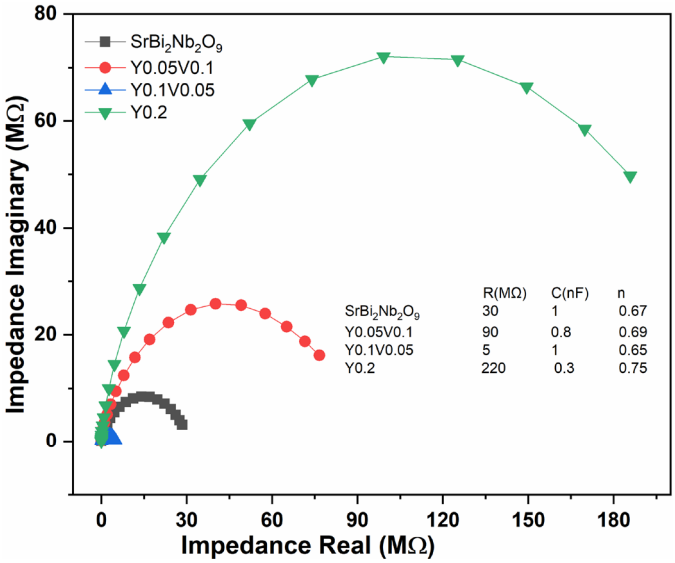

Fig. 7. Nyquist diagram at room temperature of $SrBi_{2-x}Y_xNb_{2-y}V_yO_9$ ($0 \le x \le 0.2$ and $0 \le y \le 0.2$) ceramics

4. Conclusion

In this work, Molten salt was used for synthesizing $SrBi_{2-x}Y_xNb_{2-y}V_yO_9$ ($0 \le x \le 0.2$ and $0 \le y \le 0.2$) ceramics. Under the optimized experimental conditions, the annealing temperature was not optimized to remove the microstrain. FTIR spectroscopy results showed a strong band around 612 cm^{-1}, characteristic of the Aurivillius, they reveal also a slight decrease of this band (612 cm^{-1}) due to the presence of dopants. SEM observations showed that the molten salt process made up a plate-like bonded particles shape. The electrical and dielectric studies show that impedance, dielectric constants and dielectric loss tangent of the ceramics were heterogeneous depending on the amount of doping. The codoping increases the dielectric loss tangent of the $SrB_{1.9}Y_{0.1}Nb_{1.95}V_{0.05}O_9$ (Y0.1V0.05) ceramic. Further, losses were decreased significantly in the case of $SrBi_{1.8}Y_{0.2}Nb_2O_9$ (Y0.2) ceramic. In essence, the $SrB_{1.9}Y_{0.1}Nb_{1.95}V_{0.05}O_9$ (Y0.1V0.05) sample makes up the highest efficient charge transfer, followed by $SrBi_{1.8}Y_{0.2}Nb_2O_9$ (Y0.2) sample representing the lowest.

REFERENCES

[1] V.G. Vlasenko, A.T. Shuvaev, D.S. Drannikov, Powder Diffr. **20**, 1-6 (2005).
[2] J.F. Scott, C.A. Paz De Araujo, Science **246**, 1400-1405 (1989).
[3] S. Eränen, Micro Nano Technol. 133-213 (2020).
[4] J.D. Bobic, M.M. Vijatovic Petrovic, B.D. Stojanovic, Met. Oxides 233-249 (2018).
[5] T. Asai, E.R. Camargo, M. Kakihana, M. Osada, J. Alloys Compd. **309**, 113-117 (2000).
[6] T. Kimura, Adv. Ceram. - Synth. Charact. Process. Specif. Appl. (2011).
[7] S.K. Gupta, Y. Mao, Prog. Mater. Sci. 00734 (2020).
[8] B.-R. Li, X.-T. Liu, Y.-S. Zheng, H.-B. Chang, Adv. Mater. Res. **177**, 12-15 (2011).
[9] B.H. Venkataraman, K.B.R. Varma, J. Mater. Sci. Mater. Electron. **16**, 335-344 (2005).
[10] S.M. Blake, M.J. Falconer, M. Mccreedy, P. Lightfoot **9**, 1609-1613 (1997).
[11] S.Y. Cho, G.P. Choi, D.H. Jeon, T.A. Johnson, M.K. Lee, G.J. Lee, S.D. Bu, Curr. Appl. Phys. (2015).
[12] J. Zhou, J. Adv. Ceram. **1**, 89-99 (2012).
[13] D. Priyadarsini Jena, B. Mohanty, R.K. Parida, B.N. Parida, N.C. Nayak, Mater. Chem. Phys. **243**, 122527 (2020).
[14] V. Purohit, R.N.P. Choudhary, Mater. Chem. Phys. **256**, (2020).
[15] O. Rosales-González, F. Pedro-García, F. Sánchez-De Jesús, A. Barba-Pingarrón, M. Ramírez-Cardona, A.M. Bolarín-Miró, Ceram. Int. (2020).